Brain hypoxia mapping in acute stroke: back-to-back T2' MR versus ^{18}F-fluoromisonidazole PET in rodents

Ulf Jensen-Kondering, MD[1,2,3], Roido Manavaki, PhD[4]*, Sohail Ejaz, PhD[1]*, Stephen J Sawiak, PhD[2], T. Adrian Carpenter, PhD[2], Tim D. Fryer, PhD[2], Franklin I. Aigbirhio, PhD[2], David J. Williamson, PhD[2], Jean-Claude Baron, ScD[1,5]

*: these authors share 2nd authorship

1: Stroke Research Group, Department of Clinical Neurosciences, University of Cambridge, UK

2: Wolfson Brain Imaging Centre, Department of Clinical Neurosciences, University of Cambridge, Cambridge, UK

3. Department of Radiology and Neuroradiology, University Medical Center Schleswig-Holstein, Kiel, Germany

4: Department of Radiology, University of Cambridge, Cambridge, UK

5: INSERM U894, Université Paris Descartes, Hôpital Sainte-Anne, Paris, France

Corresponding author:

Jean-Claude Baron, INSERM U894, 2ter rue d'Alésia, 75014 Paris, France

tel: (33) (0)1 40788626; fax: (33) (0)1 45807293; email: jean-claude.baron@inserm.fr

Cover title: MR-based T2' versus PET-based hypoxia imaging

Word count: 4,748

Conflict-of-interest: all authors declare no conflict of interest.

Abstract

Background. Mapping the hypoxic brain in acute ischemic stroke has considerable potential for both diagnosis and treatment monitoring. PET using ^{18}F-fluoro-misonidazole (FMISO) is the reference method, however it lacks clinical accessibility and involves radiation exposure. MR-based T2' mapping may identify tissue hypoxia and holds clinical potential. However, its validation against FMISO imaging is lacking. Here we implemented back-to-back FMISO-PET and T2' MR in rodents subjected to acute middle cerebral artery occlusion (MCAo). For direct clinical relevance, regions-of-interest (ROIs) delineating reduced T2' signal areas were manually drawn.

Methods. Wistar rats were subjected to filament MCAo, immediately followed by intravenous FMISO injection. Multi-echo T2 and T2* sequences were acquired twice during FMISO brain uptake, interleaved with diffusion-weighted imaging. Perfusion-weighted MR was also acquired whenever feasible. Immediately following MR, PET data reflecting the history of FMISO brain uptake during MR acquisition were acquired. T2' maps were generated voxel-wise from T2 and T2*. Two raters independently drew T2' lesion ROIs. FMISO uptake and perfusion data were obtained within T2' consensus ROIs, and their overlap with the automatically-generated FMISO lesion and ADC lesion ROIs was computed.

Results. As predicted, consensus T2' lesion ROIs exhibited high FMISO uptake as well as substantial overlap with the FMISO lesion and significant hypoperfusion, but only small overlap with the ADC lesion. Overlap of the T2' lesion ROIs between the two raters was ~50%.

Conclusions. This study provides formal validation of T2' to map non-core hypoxic tissue in acute stroke. T2' lesion delineation reproducibility was suboptimal, reflecting unclear lesion borders.

Key Words: positron emission tomography; cerebral ischemia; MRI; brain imaging; stroke; FMISO

Introduction

In acute ischemic stroke, imaging the hypoxic brain at risk of impending infarction is an important goal (1). PET-based methods to indirectly map brain hypoxia using oxygen-15 labelled compounds are complex, expensive and scarcely-available (2). The direct PET hypoxia tracer ^{18}F-fluoro-misonidazole (FMISO) accumulates over time in hypoxic but non necrotic brain areas thanks to irreversible covalent trapping of its reduced form to cell organelles (3), and has been extensively used in acute ischemic stroke studies, both pre-clinical (4-8) and clinical(9-16). However, FMISO PET remains poorly accessible in the acute clinical setting, and in addition involves radiation exposure. More widely accessible, non-invasive approaches to map acute brain hypoxia are therefore highly desirable. Recent efforts have aimed to develop various MR-based approaches to directly map tissue hypoxia (17, 18), all based on the T2* susceptibility effect reflecting the local deoxyhemoglobin/oxyhemoglobin ratio. Among these, T2' mapping is particularly promising as it provides direct information on local deoxyhemoglobin concentration, and hence should be sensitive to tissue hypoxia.

Although previous work in stroke patients and rodent models found T2' reductions in hypoperfused areas and within apparent diffusion coefficient (ADC) lesions, consistent with tissue hypoxia (19-24), no direct validation of T2' imaging against PET has been reported so far. Furthermore, all the above experimental and clinical studies reported T2' values within hypoperfused or ADC lesion regions-of-interest (ROIs), but did not directly

address the clinically relevant question whether reduced T2' signal, assumed to represent tissue hypoxia, can be reliably delineated by visual inspection of T2' maps.

Aims and Hypothesis

The present PET and MR back-to-back study therefore aimed to directly test the hypothesis that T2' lesions truly reflect acute tissue hypoxia. To this end, we assessed in a rodent stroke model whether areas of reduced T2' signal i) exhibit high FMISO uptake; and ii) topographically match to FMISO hypoxia lesions. The imaging protocol exploited the specific feature of intravenously administered FMISO to slowly accumulate in hypoxic tissue over 2.5hrs. Accordingly, MR data acquisition was carried out whilst FMISO accumulated in hypoxic tissue, and actual PET data acquisition was carried out once MR acquisition was complete. To test the above hypothesis, we determined if FMISO uptake is effectively higher within the visually-delineated T2' lesion ROIs, and how well the latter overlaps FMISO lesions. Because the ischemic core is expected to exhibit only mild residual hypoxia, we also predicted that the T2' lesion ROI would only marginally overlap with the apparent diffusion coefficient (ADC) lesion ROI. In addition, as an ancillary substudy, we aimed to confirm the presence of hypoperfusion within the T2' lesion ROIs in our setting. Finally, to assess reliability, we determined the inter-rater reproducibility in T2' lesion ROI delineation.

Material and Methods

This study was approved by the University of Cambridge Ethical Review Panel, who required that the study be designed so as to keep the number of animals to a minimum, yet sufficient to obtain meaningful results, in accordance with the legislation of UK Animals Scientific Procedures Act 1986. Accordingly, five animals are considered sufficient to provide a proof-of-concept study addressing a single, well-defined hypothesis. The large human resources and costs involved in the present complex studies was another constraint. Animal experiments complied with the ARRIVE guidelines. As no early death or other complications occurred, all five experimental subjects are reported.

Subjects

Adult male Wistar rats (n=5, 385 ± 22g) were used. This strain was selected because it has slower stroke evolution than other strains (25), which was relevant for this study where MR and PET data were to be compared over 2.5hrs after middle cerebral artery occlusion (MCAo), see protocol below.

Surgical procedures

Under isoflurane anesthesia, spontaneously breathing rats underwent filament MCAo (**Supplemental Methods**). Clear ischemic lesions were consistently present on diffusion-weighted MR (DWI), FMISO PET and TTC staining (see Results).

Imaging protocol

The imaging protocol is detailed in the **Supplemental Methods**. In brief, immediately following MCAo (median 3mins, range 1-7mins), the anesthetized animal was intravenously administered ^{18}F-FMISO as a slow bolus, and transferred to the 4.7T MR scanner. Median time from FMISO injection to start of MR acquisition was 12mins (range 10-15mins).

MRI

The protocol timelines are depicted in **Figure 1**, and detailed in **Supplemental Methods**. Following a T2-weighted (T2w) scan for coregistration purposes, the following sequences were acquired twice directly back-to-back (to be referred to as 'time point 1' and 'time point 2'): DWI, multiecho T2 and multiecho T2*. Overall scanning time for each block was 44min 26s. In three animals, dynamic susceptibility contrast (DSC) perfusion-weighted MRI was acquired immediately after the second MR block.

PET

Once MR acquisition complete, the animal was transferred to a microPET. FMISO emission data were acquired from 120 to 150min post-injection, followed by transmission data. See **Supplemental Methods** for details. The attenuation-corrected FMISO image was converted to a standardised uptake value (SUV) image, using the injected activity and animal weight.

Tetrazolium chloride (TTC)

Immediately after completion of PET scanning, TTC staining was carried as detailed in **Supplemental Methods**. ROIs delineating the lesion across all brain sections were independently drawn by two observers using ImageJ, and any disagreement subsequently resolved by consensus.

MR image processing

T2' maps

T2' maps were generated as detailed in **Supplemental Methods**. This process yielded maps of absolute T2' for each rat and each MR acquisition block. Image coregistration procedures are detailed in **Supplemental Methods.**

ROI definition and data analysis

For each time point, T2' lesion ROIs, i.e., hypointense areas compared to contralateral corresponding regions, were independently delineated on the T2' maps by two observers (**Supplemental Methods)**. Consensus ROIs were used for further calculations and comparisons.

ADC lesion ROIs were automatically generated using $ADC<530*10^{-6}mm^2/s$ (26). Finally, FMISO lesion ROIs were automatically derived on the SUV images according to an automated statistical voxel-based method detailed elsewhere (8), applying p=0.01 as cut-off.

Dimensionless weighted mean Affected/Unaffected side-to-side ratios for the above variables were calculated following generation of Mirror ROIs on the contralesional hemisphere **(Supplemental Methods).**

Perfusion data analysis

MR-DSC data were analyzed using standard methodology (**Supplemental Methods**) to generate quantitative CBF, CBV, MTT and TTP maps.

Statistical analysis

Inter-observer agreement was assessed using the percent geometrical overlap between the T2' ROIs from both observers, calculated for each time point as the area of intersection between, divided by the average of, the two ROIs, multiplied by 100; a weighted average % overlap was then computed across slices. The closer this index is to 100 % the more similar the two ROIs are. The overlap between the T2' and ADC ROIs, and that between the T2' and FMISO lesion ROIs, was expressed relative to the T2' lesion ROI volume. The overlap between the TTC ROIs from the two observers was computed as with the T2' lesion ROIs. Finally, CBF, CBV, MTT and TTP ratios within the time-point 2 T2' lesion ROIs versus mirror ROIs were computed.

Given the small sample not permitting Wilcoxon non-parametric tests, parametric tests were used throughout. Correction for multiple tests was not considered given the biologically straightforward hypotheses. Two-tailed $p<0.05$ was considered significant

save for the perfusion data where one-tailed p was used given the sample size and confirmatory aim only (n=3).

Results

Figure 2 illustrates typical imaging findings from this study.

Inter-observer agreement

The mean (±SD) % overlap in T2' lesion ROIs between the two observers was 66 ± 29% and 43 ± 35% at time-points 1 and 2, respectively. **Supplemental Figure 1** illustrates examples of original and consensus T2' lesion ROIs.

FMISO SUV in T2' consensus ROIs

The mean FMISO SUV value within the T2' consensus ROI was almost twice higher than in mirror ROI (**Table 1**), which was statistically significant at time-point 2 and not quite at time-point 1 (no significant differences between time points). Also shown for the sake of completeness are the SUV values within the ADC ROI, which were higher than in the T2' lesion ROI but not significantly so.

Volume of the T2' consensus, FMISO and ADC ROIs

The volumes of the T2' consensus and ADC ROIs for each rat and each time-point are shown in **Table 2**, together with the FMISO ROI volumes.

Overlap between the T2' consensus ROI and the FMISO lesion ROI

Excluding the rat with no T2' ROI at time-point 1 (Table 2), the % overlap between the consensus T2' lesion ROI and the FMISO lesion ROI ranged from 0 (for the two smallest T2' ROIs) to 96%, with a mean (± 1SD) of 44 (± 39.6%) and 55.6 (± 36.2%) at time- points 1 and 2, respectively.

T2' consensus ROI versus ADC ROI

As predicted, the overlap between the T2' consensus ROI and the ADC ROI was very small at both time points, even excluding the three zero volumes, and ranged from 0 for the smallest T2' or ADC lesions to 23% for the largest ADC lesion, with means (± 1SD) of 1.0% (± 1.7%) and 11.0% (± 9.2%), respectively (not significantly different from each other).

Perfusion within the T2' lesion ROIs

As expected, the CBF and CBV ratios within the T2' consensus lesion ROIs were significantly reduced, and the TTP and MTT ratios significantly elevated (**Table 3**).

TTC staining

All animals displayed a TTC lesion (**Figure 3)**. Inter-observer agreement between lesions was 76.6%. The volumes of the TTC lesion consensus ROIs are shown in Table 2.

Discussion

Consistent with our hypothesis, FMISO uptake was higher (~2-fold) in the T2' lesion ROI relative to its mirror ROI, and there was substantial (~50%) overlap between the T2' and FMISO lesion ROIs. These novel findings document that the T2' lesion effectively reflects acutely hypoxic tissue after stroke. Consistent with the idea that the T2' lesion is largely distinct from the ischemic core, it only slightly overlapped with the ADC lesion. Finally, consistent with previous literature, the T2' lesion ROI was clearly hypoperfused.

To allow biologically meaningful comparison of the T2' maps to the FMISO images, the T2 and T2* data were acquired at two time-points covering the early and most meaningful part of FMISO brain uptake. PET data acquisition was then carried out 120- 150min post-FMISO administration. FMISO images acquired in this time-frame represent the 'history' of FMISO uptake since tracer injection (3). Thus, the T2' and FMISO images largely covered the same period of tissue hypoxia. Note that as previously documented, marked tracer accumulation does take place in ischemic areas in spite of prevailing hypoperfusion(4). The FMISO lesion was defined using automated voxel- based statistical mapping deriving an upper threshold from FMISO uptake in the unaffected hemisphere (8), using $p<0.01$ as cut-off. Applying more stringent thresholds (e.g., 0.001 and 0.0001) in *post hoc* sensitivity analyses showed only slightly smaller overlaps, as this has only small effects on FMISO ROI volumes (8).

As hypothesized, the T2' lesion ROI showed markedly higher FMISO uptake than mirror ROIs, together with substantial overlap with the FMISO lesion. There is no previous T2'

vs PET hypoxia study for direct comparison. As also predicted based on the notion that dead or dying neurons are less hypoxic (27), the T2' lesion overlapped little with the ADC lesion. Thus, our data directly establish that the T2' lesion effectively reflects acutely hypoxic, but mainly non-core tissue (see Figure 2).

The incomplete overlap between the T2' and FMISO lesion ROIs, with the latter larger than the former (Table 2, Figure 2), may in part relate to intrinsic biological differences between these two hypoxia markers. While T2' reflects the local balance between oxygenated and reduced hemoglobin (17), FMISO trapping expresses covalent binding to intracellular molecules taking place only in hypoxic conditions (3). A recent clinical study reported high FMISO uptake in the core diffusion lesion (9), as also true here (Table 1; Figure 2), and previous rodent studies found high FMISO uptake in mildly ischemic areas (8). Thus, FMISO trapping appears to take place not just in the ischemic penumbra but also to some extent in the early core and oligemia.

That in our study the T2' lesions were hypoperfused is consistent with sudstantial previous evidence. Thus, hypoperfused areas were found to have reduced T2' values in one previous rat study which presented images but no actual data (21) as well as reduced R2' values in a monkey study (24) (note: R2' = 1/T2'). In another rat study assessing T2' and perfusion within the DWI lesion at 90min following 60min MCAo(22), T2' tended to decrease in persistently hypoperfused DWI lesions. Two clinical studies in acute stroke (19, 20) also reported significantly reduced T2' within hypoperfused ROIs. Finally, in patients with high-grade carotid artery stenosis or occlusion, Seiler et al (23) also found

reduced T2' within chronically oligemic areas. Importantly, however, none of the above studies actually delineated low T2' lesions as done here. Of note, local increases in cerebral blood volume (CBV) are known to potentially cause artefactual reductions in T2' (17, 28). However, in our study CBV was reduced, not increased, within the T2' lesions, consistent with previous animal imaging studies consistently showing reduced CBV within the acutely ischemic area, be it using PET (29-31), CT perfusion (32), MR DSC perfusion (33), steady-state MR susceptibility imaging with ultra-small iron-oxide particles (34, 35) or functional ultrasound (36).

The overlap in T2' lesion ROIs independently drawn by the two observers was suboptimal, suggesting that although T2' lesions are conspicuous, their boundaries may be difficult to delineate (see Figure 2). This cannot be explained by inadequate MCAo as shown by the presence of ADC, FMISO and TTC lesions in all subjects, but is consistent with a clinical study showing limited inter-rater reproducibility in T2' lesion visual identification (37). Ill-defined borders of T2' lesions also appeared to affect previously published T2' maps both from animal studies (21, 22, 24) and acute stroke patients (20, 38), even after head motion correction (19). This feature might be related to the intrinsic nature of the T2' signal, together with local changes in CBV and the voxel-based divisions and subtractions involved in generating T2' maps (see Supplemental Methods).

The main advantage of T2' over T2* is its independence from T2 effects, and hence from vasogenic edema (17), which can develop rapidly after experimental stroke (39), with T2-weighted scans becoming positive as early as 90-120mins post-stroke in rodents (40) and

humans (41). For the sake of completeness, we visually compared post-hoc the T2* to the T2' maps, which did not reveal more clearly visible lesions (data not shown; see Figure 2 as example). To assess whether our findings are specific to T2', we also generated R2' maps (see above), and duplicated the entire visual and ROI analysis, which as expected revealed essentially identical results (data not shown; see Figure 2 as an illustration).

As we used a small sample, our findings need independent replication. However, carrying out both PET and MR after MCAo in the rodent represents a major challenge, and our study is unique. The recent advent of hybrid PET/MR scanners should resolve some of the technical obstacles involved (42).

In conclusion, this study validated T2' as a marker of acute brain hypoxia against gold-standard PET, which has important clinical implications. Reproducibility of T2' lesion delineation was suboptimal, but further studies should determine if this shortcoming can be overcome by optimizing image acquisition and processing and/or observer experience.

Acknowledgements: None.

Sources of Funding: This study was funded by an EU Grant (EUSTROKE Health-F2-2008-2022131). DJW was funded by an MRC collaborative grant (G0600986), RM by the NIHR Cambridge Biomedical Research Centre, and UJK by a fellowship from the Deutsche Forschungsgemeinschaft (Je 598/1-1).

Author contribution:

- UJK: study concept, experiments, data analysis, manuscript drafting

- RM: data analysis
- SE: experiments, data analysis
- SJS: experiments, data analysis
- TAC: protocol, experiments
- TDF: protocol, experiments, data analysis
- FIA: experiments
- DJW: animal license holder, experiments
- JCB: study concept, protocol, funding, manuscript revisions and final version

Literature cited

1. Moustafa RR, Baron JC. Clinical review: Imaging in ischaemic stroke--implications for acute management. Critical care (London, England) 2007;11(5):227.
2. Muir KW, Buchan A, von Kummer R, Rother J, Baron JC. Imaging of acute stroke. Lancet Neurol 2006;5(9):755-68.
3. Takasawa M, Moustafa RR, Baron JC. Applications of nitroimidazole in vivo hypoxia imaging in ischemic stroke. Stroke 2008;39(5):1629-37.
4. Takasawa M, Beech JS, Fryer TD, et al. Imaging of brain hypoxia in permanent and temporary middle cerebral artery occlusion in the rat using 18F-fluoromisonidazole and positron emission tomography: a pilot study. J Cereb Blood Flow Metab 2007;27(4):679-89.
5. Spratt NJ, Ackerman U, Tochon-Danguy HJ, Donnan GA, Howells DW. Characterization of fluoromisonidazole binding in stroke. Stroke 2006;37(7):1862-7.
6. Spratt NJ, Donnan GA, Howells DW. Characterisation of the timing of binding of the hypoxia tracer FMISO after stroke. Brain Res 2009; 1288:135-42.
7. Rojas S, Herance JR, Abad S, et al. Evaluation of hypoxic tissue dynamics with 18F-FMISO PET in a rat model of permanent cerebral ischemia. Mol Imaging Biol 2011;13(3):558-64.
8. Takasawa M, Beech JS, Fryer TD, et al. Single-subject statistical mapping of acute brain hypoxia in the rat following middle cerebral artery occlusion: a microPET study. Exp Neurol 2011;229(2):251-8.
9. Alawneh JA, Moustafa RR, Marrapu ST, et al. Diffusion and perfusion correlates of the 18F-MISO PET lesion in acute stroke: pilot study. Eur J Nucl Med Mol Imaging 2014;41(4):736-44.
10. Falcao AL, Reutens DC, Markus R, et al. The resistance to ischemia of white and gray matter after stroke. Ann Neurol 2004;56(5):695-701.
11. Markus R, Donnan GA, Kazui S, et al. Statistical parametric mapping of hypoxic tissue identified by [(18)F]fluoromisonidazole and positron emission tomography following acute ischemic stroke. Neuroimage 2002;16(2):425-33.
12. Markus R, Reutens DC, Kazui S, et al. Topography and temporal evolution of hypoxic viable tissue identified by 18F-fluoromisonidazole positron emission tomography in humans after ischemic stroke. Stroke 2003;34(11):2646-52.
13. Markus R, Reutens DC, Kazui S, et al. Hypoxic tissue in ischaemic stroke: persistence and clinical consequences of spontaneous survival. Brain 2004;127(Pt 6):1427-36.
14. Read SJ, Hirano T, Abbott DF, et al. The fate of hypoxic tissue on 18F-fluoromisonidazole positron emission tomography after ischemic stroke. Ann Neurol 2000;48(2):228-35.
15. Read SJ, Hirano T, Abbott DF, et al. Identifying hypoxic tissue after acute ischemic stroke using PET and 18F-fluoromisonidazole. Neurology 1998;51(6):1617-21.

16. Lee GH, Kim JS, Oh SJ, Kang DW, Kim JS, Kwon SU. (18)F-fluoromisonidazole (FMISO) Positron Emission Tomography (PET) Predicts Early Infarct Growth in Patients with Acute Ischemic Stroke. J Neuroimaging 2015;25(4):652-5.
17. Jensen-Kondering U, Baron JC. Oxygen imaging by MRI: can blood oxygen level-dependent imaging depict the ischemic penumbra? Stroke 2012;43(8):2264-9.
18. Yablonskiy DA, Sukstanskii AL, He X. Blood oxygenation level-dependent (BOLD)-based techniques for the quantification of brain hemodynamic and metabolic properties - theoretical models and experimental approaches. NMR Biomed 2013;26(8):963-86.
19. Bauer S, Wagner M, Seiler A, et al. Quantitative T2'-mapping in acute ischemic stroke. Stroke 2014;45(11):3280-6.
20. Geisler BS, Brandhoff F, Fiehler J, et al. Blood-oxygen-level-dependent MRI allows metabolic description of tissue at risk in acute stroke patients. Stroke 2006;37(7):1778-84.
21. Grune M, van Dorsten FA, Schwindt W, Olah L, Hoehn M. Quantitative T*(2) and T'(2) maps during reversible focal cerebral ischemia in rats: separation of blood oxygenation from nonsusceptibility-based contributions. Magn Reson Med 1999;42(6):1027-32.
22. Jensen UR, Liu JR, Eschenfelder C, et al. The correlation between quantitative T2' and regional cerebral blood flow after acute brain ischemia in early reperfusion as demonstrated in a middle cerebral artery occlusion/reperfusion model of the rat. J Neurosci Methods 2009;178(1):55-8.
23. Seiler A, Jurcoane A, Magerkurth J, et al. T2' imaging within perfusion-restricted tissue in high-grade occlusive carotid disease. Stroke 2012;43(7):1831-6.
24. Zhang J, Chen YM, Zhang YT. Blood-Oxygenation-Level-Dependent-(BOLD-) Based R2' MRI Study in Monkey Model of Reversible Middle Cerebral Artery Occlusion. J Biomed Biotechnol 2011; 2011:318346.
25. Letourneur A, Freret T, Roussel S, et al. Maternal hypertension during pregnancy modifies the response of the immature brain to hypoxia-ischemia: sequential MRI and behavioral investigations. Experimental neurology 2012;233(1):264-72.
26. Meng X, Fisher M, Shen Q, Sotak CH, Duong TQ. Characterizing the diffusion/perfusion mismatch in experimental focal cerebral ischemia. Ann Neurol 2004;55(2):207-12.
27. Furlan M, Marchal G, Viader F, Derlon JM, Baron JC. Spontaneous neurological recovery after stroke and the fate of the ischemic penumbra. Ann Neurol 1996;40(2):216-26.
28. Seiler A, Deichmann R, Pfeilschifter W, Hattingen E, Singer OC, Wagner M. T2-Imaging to Assess Cerebral Oxygen Extraction Fraction in Carotid Occlusive Disease: Influence of Cerebral Autoregulation and Cerebral Blood Volume. PLoS One 2016;11(8): e0161408.
29. Heiss WD, Graf R, Wienhard K, et al. Dynamic penumbra demonstrated by sequential multitracer PET after middle cerebral artery occlusion in cats. Journal of cerebral blood flow and metabolism: official journal of the International Society of Cerebral Blood Flow and Metabolism 1994;14(6):892-902.
30. Pappata S, Fiorelli M, Rommel T, et al. PET study of changes in local brain hemodynamics and oxygen metabolism after unilateral middle cerebral artery occlusion

in baboons. Journal of cerebral blood flow and metabolism: official journal of the International Society of Cerebral Blood Flow and Metabolism 1993;13(3):416-24.
31. Young AR, Sette G, Touzani O, et al. Relationships between high oxygen extraction fraction in the acute stage and final infarction in reversible middle cerebral artery occlusion: an investigation in anesthetized baboons with positron emission tomography. J Cereb Blood Flow Metab 1996;16(6):1176-88.
32. McLeod DD, Parsons MW, Hood R, et al. Perfusion computed tomography thresholds defining ischemic penumbra and infarct core: studies in a rat stroke model. International journal of stroke: official journal of the International Stroke Society 2015;10(4):553-9.
33. Sakoh M, Rohl L, Gyldensted C, Gjedde A, Ostergaard L. Cerebral blood flow and blood volume measured by magnetic resonance imaging bolus tracking after acute stroke in pigs: comparison with [(15)O]H(2)O positron emission tomography. Stroke 2000;31(8):1958-64.
34. Quast MJ, Wei J, Huang NC, et al. Perfusion deficit parallels exacerbation of cerebral ischemia/reperfusion injury in hyperglycemic rats. Journal of cerebral blood flow and metabolism: official journal of the International Society of Cerebral Blood Flow and Metabolism 1997;17(5):553-9.
35. Zaharchuk G, Yamada M, Sasamata M, Jenkins BG, Moskowitz MA, Rosen BR. Is all perfusion-weighted magnetic resonance imaging for stroke equal? The temporal evolution of multiple hemodynamic parameters after focal ischemia in rats correlated with evidence of infarction. Journal of cerebral blood flow and metabolism: official journal of the International Society of Cerebral Blood Flow and Metabolism 2000;20(9):1341-51.
36. Brunner C, Isabel C, Martin A, et al. Mapping the dynamics of brain perfusion using functional ultrasound in a rat model of transient middle cerebral artery occlusion. J Cereb Blood Flow Metab 2017;37(1):263-76.
37. Fiehler J, Geisler B, Siemonsen S, et al. [Visual rating of T2'-blood-oxygen-level-dependent magnetic resonance imaging in acute stroke patients--a pilot study]. Rofo 2007;179(1):17-20.
38. Siemonsen S, Fitting T, Thomalla G, et al. T2' imaging predicts infarct growth beyond the acute diffusion-weighted imaging lesion in acute stroke. Radiology 2008;248(3):979-86.
39. Shi Y, Zhang L, Pu H, et al. Rapid endothelial cytoskeletal reorganization enables early blood-brain barrier disruption and long-term ischaemic reperfusion brain injury. Nat Commun 2016; 7:10523.
40. Hoehn-Berlage M, Eis M, Back T, Kohno K, Yamashita K. Changes of relaxation times (T1, T2) and apparent diffusion coefficient after permanent middle cerebral artery occlusion in the rat: temporal evolution, regional extent, and comparison with histology. Magn Reson Med 1995;34(6):824-34.
41. Thomalla G, Cheng B, Ebinger M, et al. DWI-FLAIR mismatch for the identification of patients with acute ischaemic stroke within 4.5 h of symptom onset (PRE-FLAIR): a multicentre observational study. Lancet Neurol 2011;10(11):978-86.
42. Werner P, Saur D, Zeisig V, et al. Simultaneous PET/MRI in stroke: a case series. Journal of cerebral blood flow and metabolism: official journal of the International Society of Cerebral Blood Flow and Metabolism 2015;35(9):1421-5.

Figure legends:

Figure 1

Protocol timelines starting with the middle cerebral artery occlusion (MCAo) and finishing with tetrazolium chloride (TTC) staining of brain sections (left to right). Total duration from the beginning of MR data acquisition to the end of emission PET data acquisition was 150mins. Legend: LR: low resolution; HR: high resolution; DWI: diffusion-weighted imaging; PWI: perfusion-weighted imaging; TS: transmission scan.

Figure 2

Representative T2, T2*, T2' and ADC maps of the same coronal brain section from rat #5, obtained at time-points 1 (top) and 2 (bottom), also showing for the latter the CBF, CBV and TTP images (MTT image not shown as almost identical to the TTP image). Also shown are the corresponding R2' images obtained by inverting the T2' images. To the right is shown the coregistered FMISO SUV image, acquired 120-150mins after tracer injection (see Figure 1) but representing the 'history' of tracer behavior in brain since administration (see Discussion). The high FMISO uptake area (in yellow) reflects tracer retention in hypoxic areas. The images depict reduced T2' (and increased R2') signal in the affected MCA territory at both time points, geometrically matching the hypoperfused areas. There is substantial overlap of the T2' lesion with the FMISO high uptake region, and little overlap with the ADC lesion. These images also illustrate the lack of definite borders of the T2' lesions. Note the good quality of the original T2 and

T2* images. Next to the CBF, CBV and TTP images are shown pseudocolor scales used to display these images, in units of mls/100g.min, mls/100g and seconds, respectively. The monocolor scale (in SUV units; see Methods) used to display the FMISO image is shown below the latter. See Tables 1 and 3 for the average FMISO and perfusion values within the T2' lesion ROIs.

Figure 3

Representative TTC stained coronal sections from the five animals, consistently displaying an acute ischemic lesion. The yellow outlines represent the consensus TTC lesion ROIs.

Tables

Table 1: Mean (± SD) FMISO SUV (% injected dose/kg weight) within the T2' and ADC lesion ROIs and their respective mirror ROIs for each time-point.

	Time-point 1	**p***	**Time-point 2**	**p***
T2' ROI	0.91 ± 0.32	0.080	0.94 ± 0.22	0.009
Mirror ROI	0.56 ± 0.07		0.57 ± 0.08	
ADC ROI	1.16 ± 0.19	0.002	1.18 ± 0.11	0.001
Mirror ROI	0.57 ± 0.09		0.58 ± 0.09	

*: two-tailed paired t-tests comparing FMISO SUV in the lesion ROI to that in its mirror ROI

Table 2. Individual rat volumes (mm^3) for the T2' consensus ROI and ADC ROI at both time-points, and for the FMISO and TTC ROIs.

Rat #	Time-point 1		Time-point 2			
	T2'	**ADC**	**T2'**	**ADC**	**FMISO**	**TTC**
1	94	5.0	132.2	42.5	303.5	166.9
2	0	31.4	130.3	21.3	249.2	142.3
3	6.6	0	25.8	0	64.3	32.1
4	102.5	0.3	68.1	9.3	257.6	259.6
5	74.2	1.8	112.1	10.1	170.7	106.1

Table 3: Perfusion values in the T2' lesion consensus ROI relative to the contralateral mirror ROI for time-point 2 (unitless ratios).

	CBF	CBV	MTT	TTP
Ratio values	0.52 ± 0.13	0.57 ± 0.14	1.16 ± 0.26	1.21 ± 0.06
P values	p=0.024*	p=0.034*	p=0.016*	p=0.029*

*: $p < 0.05$ (one-tailed t-test against unity, n=3)

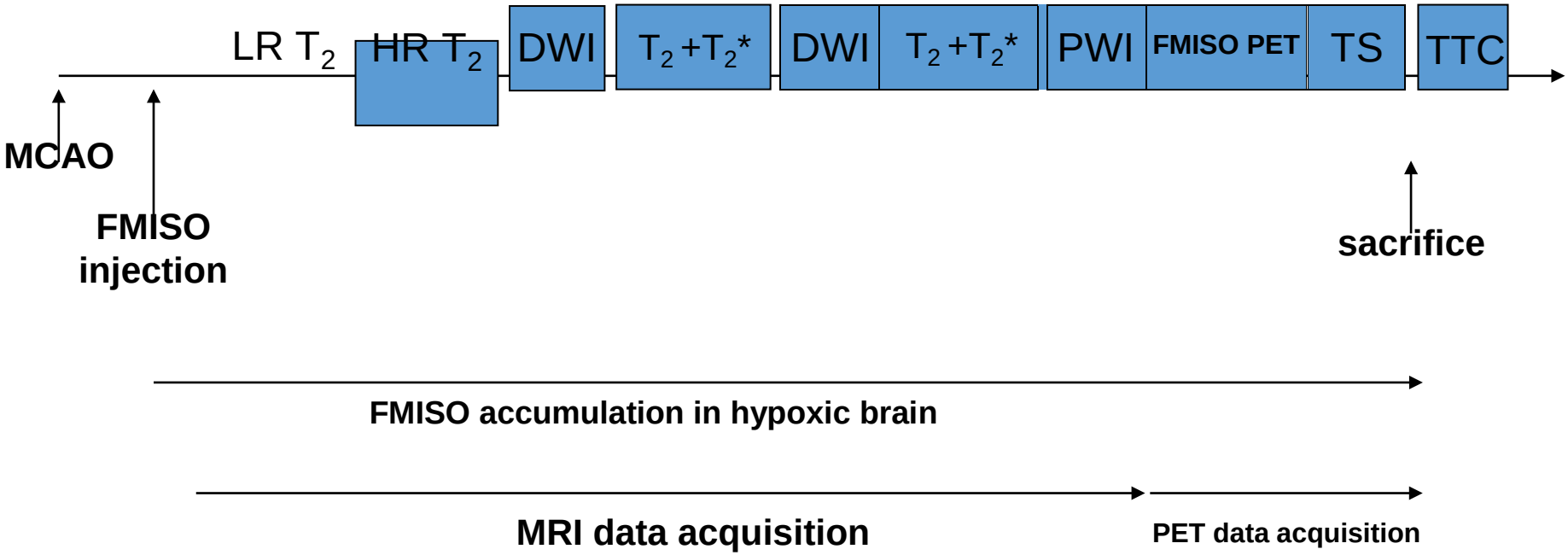
LR T_2
HR T_2
DWI
T_2 +T_2*
DWI
T_2 +T_2*
PWI
FMISO PET
TS
TTC
MCAO
FMISO injection
sacrifice
FMISO accumulation in hypoxic brain
MRI data acquisition
PET data acquisition

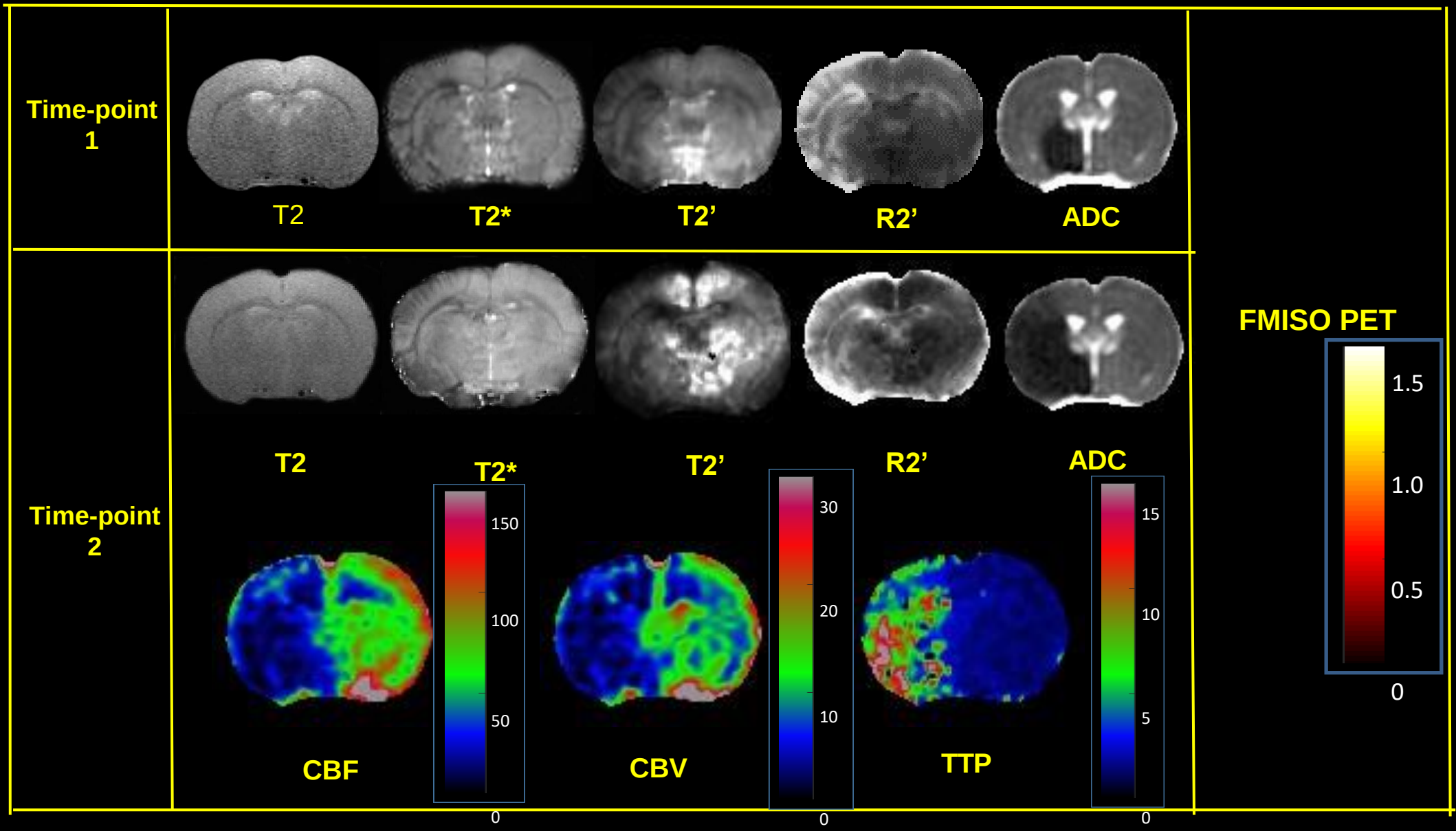
Time-point 1
T2
T2*
T2'
R2'
ADC
Time-point 2
T2
T2*
T2'
R2'
ADC
150
100
50
0
30
20
10
0
15
10
5
0
CBF
CBV
TTP
FMISO PET
1.5
1.0
0.5
0

Figure 3

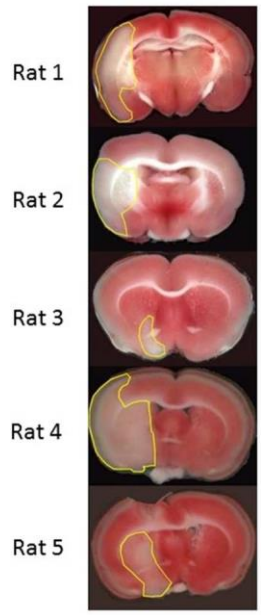

Figure 3
Representative TTC stained coronal sections from the five animals, consistently displaying an acute ischemic lesion. The yellow outlines represent the consensus TTC lesion ROIs.

254x190mm (96 x 96 DPI)